ingegneria sismica
International Journal of Earthquake Engineering
Anno XLIII - Num. 2 - 2026

Total-Focusing Technology for Subtle Defect Detection in Ceramic Sleeves Based on Phase Coherence and dB Amplitude Enhancemen

Kunnian Pan[1], *Kaida Feng*[1], *Xisheng Guan*[1], *Bin Shao*[2], *Chunhua Fang*[2,*] *and Zekun Zheng*[2]

[1] Guangdong Power Grid Yangjiang Power Supply Company, No. 110, Mojiang Road, Yangjiang, Guangdong, 529500, China
[2] College of Electricity and New Energy, China Three Gorges University, No. 8, Daxue Road, Yichang, Hubei 443002, China

SUMMARY: *To address the challenge of detecting subtle internal defects in ceramic sleeves, this paper integrates Phase Coherence Imaging (PCI), dB amplitude enhancement (dB), and the Total-Focusing Method (TFM) to improve image precision and enhance the detectability of subtle defects within ceramic sleeves. Initially, a model of subtle defects in the ceramic sleeve was developed in COMSOL, followed by a comparative simulation to analyze the effects of various ultrasonic phased array probe parameters-such as element count, element spacing, and element frequency-on defect detection and imaging at different positions, ultimately leading to the selection of optimal probe parameters. Subsequently, a test platform for ultrasonic total-focusing detection of ceramic sleeve defects was established, and experimental validation was performed by detecting a 1mm pore defect inside the ceramic sleeve using the optimal probe parameters. Results indicate that, when using the optimal probe parameters for detecting subtle defects in ceramic sleeves, the TFM-PCI-dB method effectively reduces noise and artifacts in the image, while enhancing the amplitude at defect locations, thus making defects easier to detect. The experimental results also validate that this method enables high-precision detection of subtle defects within ceramic sleeves.*

KEYWORDS: *Ceramic Sleeve; Ultrasonic Phased Array; Total-Focusing; Subtle Defects*

1 Introduction

Ceramic sleeves are insulating containers used in electrical equipment. They are commonly employed for insulation and support in high-voltage components, such as voltage transformers, current transformers, surge arresters, capacitors, transformers, and SF6 circuit breakers [1, 2]. The insulation provided by ceramic sleeves ensures the safe operation of these devices under high-voltage conditions. However, the polycrystalline structure of ceramic material and the presence of internal micro-pores and micro-cracks pose potential risks for brittle fracture and explosion of ceramic sleeves. These issues can arise during equipment operation, under external loads, or due to pressure increases caused by internal faults, leading to the potential for breakage. The fracture of ceramic sleeve can directly cause circuit breakers or isolating switches to trip, resulting in large-scale power outages. Therefore, inspecting and identifying subtle internal defects in ceramic sleeves is critically important.

Various detection techniques, including vibration acoustic methods, ultrasonic testing, and infrared/ultraviolet detection, have been applied to defect detection in ceramic sleeves and

*fang107531@163.com
https://doi.org/10.65102/is20261021
Published: 30 April, 2026

ceramic insulators [3-5]. Infrared and ultraviolet wave technologies offer advantages such as large-area scanning and fast detection, allowing for non-contact detection, but they are highly susceptible to surface contamination, environmental conditions, and insulator temperature, as well as detection distance. Vibration acoustic detection is a simple process that can identify the presence of defects in the ceramic sleeve, but it cannot accurately determine the location or type of defect. Additionally, weather conditions (e.g., strong winds or low temperatures) can affect the ceramic sleeve's response frequency in this method. Currently, the most widely used method for ceramic sleeve defect detection is ultrasonic testing [6], which primarily includes the slope method and small-angle longitudinal wave method. However, both methods lack clear visualization, require a high level of expertise and experience from the operators, and are not effective for detecting minute defects.

Although the aforementioned detection methods are effective for certain types of defects in ceramic sleeves, their detection capabilities for subtle internal defects are limited. Therefore, this paper proposes the use of ultrasonic phased array total-focusing technology to detect internal defects in ceramic sleeves, elevating traditional one-dimensional ultrasonic testing to an intuitive two-dimensional imaging detection method. Firstly, the propagation characteristics and patterns of sound waves in ceramic sleeves are analyzed using COMSOL finite element simulation software, and the parameterized scanning function is used to perform one transmission with full reception from all elements to obtain the full matrix data of the ceramic sleeve. Additionally, the impact of different element parameters on TFM, TFM-PCI, and TFM-PCI-dB imaging is studied, and the optimal element parameters are selected to detect several typical defects in the simulated ceramic sleeve model, exploring the feasibility of this method.

2 Principles of Total-Focusing and Phase Coherence Algorithms

2.1 Total-Focusing Imaging Algorithm

The toal focusing method is a post-processing imaging algorithm based on full matrix data. For an ultrasonic phased array probe with N elements, following the excitation rule of one transmission with full reception from all elements, the full matrix data S_{ij} (where $1 \leq i \leq n$, $1 \leq j \leq n$) will be collected, consisting of N×N sets of A-scan signals. This full matrix data forms the fundamental data source for the ultrasonic total-focusing imaging algorithm, covering all wave information in the detected region [7]. The TFM divides the detection region into a grid of focal points, calculates the time delay between the the transmitting element (i) and the focus point (P); and then from the focus point (P) to the receiving element (j), based on the sound speed and sound path; then performs amplitude index summation [8]. Thus, the amplitude at the focal point ($I(x, z)$) is determined, and the same process is repeated for all focal points. Finally, imaging is performed based on the amplitude matrix. The principle of total-focusing is illustrated in equations (1) and (2).

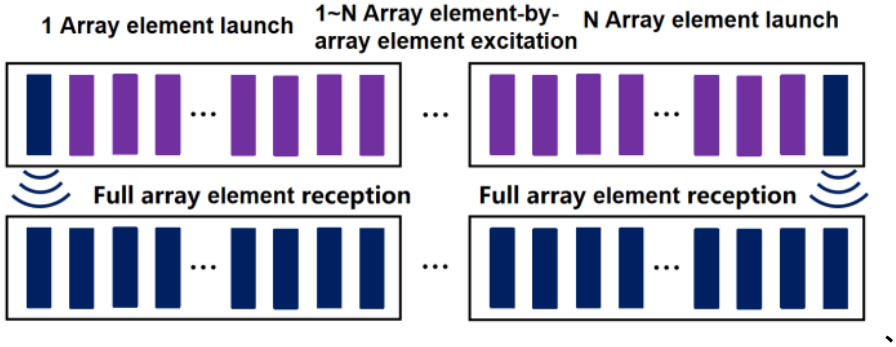

Figure 1: Schematic of full matrix data capture

	1	…	j	…	n
1	S_{11}	…	S_{1j}	…	S_{1n}
⋮	⋮	⋮	⋮	⋮	⋮
j	S_{i1}	…	S_{ij}	…	…
⋮	⋮	⋮	⋮	⋮	⋮
n	S_{n1}	…	…	…	S_{nn}

Figure 2: Schematic diagram of the captured full matrix data

$$I_p(x_p, z_p) = \sum_{i=1}^{N}\sum_{j=1}^{N} A_{ij}\left(t_{ij}(x_p, z_p)\right) \tag{1}$$

$$t_{ij}(x_p, z_p) = \frac{\left(\sqrt{(x_i - x_p)^2 + z_p^2} + \sqrt{(x_j - x_p)^2 + z_p^2}\right)}{c} \tag{2}$$

In the equations, $t_{ij}(x_p,z_p)$ represents the time required for the ultrasonic wave to propogate from element (i) to point (P), then be reflected from point (P) and received by element (j). (c) denotes the sound speed in the object being tested.

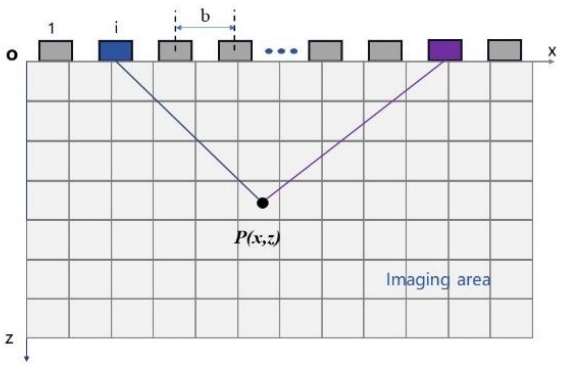

Figure 3: Schematic diagram of the total-focusing Method (TFM)

2.2 Phase Coherence and dB Amplitude Enhancement Principles

The weight factor is constructed based on the phase distribution information in the received echo signals, and then applied to the weighted reconstruction of the image [10]. In the full matrix data, the defect areas exhibit consistent phase distribution characteristics, referred to as phase alignment, which results in high phase coherence. In contrast, noise components in the echo signals exhibit scattered phase distributions and significantly lower phase coherence [11]. Based on this principle, phase information from the full matrix signals can be extracted to construct the corresponding phase coherence factor. Then, the phase coherence factor $C(x, z)$ is used to apply a weighting process to the image matrix obtained through the TFM method.

Firstly, the Hilbert transform is applied to the full matrix data using Euler's formula. The signal resulting from Hilbert transform can be written as:

$$h(t) = |h| e^{i\varphi} = |h|(\cos\varphi + j\sin\varphi) \tag{3}$$

In this equation, $|h|$ is the magnitude of the signal, and φ represents the phase angle of the signal. The phase information of the real and imaginary parts of the signal is represented by sine and cosine, respectively.

Next, the phase information and phase standard deviations, $var(\cos\varphi)$ and $var(\sin\varphi)$, corresponding to each pixel are calculated, as shown in equations (4) and (5). Based on equation (6), the Circular Coherence Factor (C_{CCF}) for each pixel is then computed and normalized. The value range of the C_{CCF} after normalization is [0, 1], where a smaller factor indicates poorer coherence, while a larger factor indicates better coherence [11]

$$\mathrm{var}(\sin\varphi(x, z, i)) = \frac{1}{N}\sum_{i=1}^{N}\sin^2\varphi - \left(\frac{1}{N}\sum_{i=1}^{N}\sin\varphi\right)^2 \tag{4}$$

$$\mathrm{var}(\cos\varphi(x, z, i)) = \frac{1}{N}\sum_{i=1}^{N}\cos^2\varphi - \left(\frac{1}{N}\sum_{i=1}^{N}\cos\varphi\right)^2 \tag{5}$$

$$C_{CCF}(x, z) = 1 - \mathrm{sqrt}[\mathrm{var}(\cos\varphi) + \mathrm{var}(\sin\varphi)] \tag{6}$$

In the equation, $var(\cos\varphi)$ and $var(\sin\varphi)$ are functions of the pixel coordinates (x, z) and the stepping position i. $sqrt[var(\cos\varphi)+var(\sin\varphi)]$ represents the phase standard deviation of each pixel in the image matrix.

Finally, the image matrix undergoes weighted reconstruction, resulting in the magnitude of the new image I_C:

$$I_C(x, z) = |C(x, z)I(x, z)| \tag{7}$$

The construction of the phase coherence factor depends on the phase standard deviation of each pixel in the image matrix [13]. Specifically, the phase coherence factor for noise pixels is low. During the weighted reconstruction process, the IC magnitude corresponding to noisy pixels will decrease, which effectively reduces the magnitude of the noise. On the contrary, for pixels with a higher phase coherence factor, the amplitude remains relatively stable after weighted reconstruction. Therefore, through the weighted reconstruction process, the noise signals in the image matrix can be effectively suppressed and removed.

The dB amplitude enhancement algorithm proceeds as follows: Firstly, an average dB threshold value (k) for the image matrix is set. Then, the dB value for each point in the image

matrix is calculated and compared with the preset threshold value (k). For all dB values less than (k), they are set to 0, while values greater than (k) remain unchanged.

3 Simulation Study on the Influence of Array Element Parameters on TFM and PCI Imaging

3.1 Simulation Model of Ultrasonic Total-Focusing Imaging for Ceramic Sleeves

A ceramic sleeve is typically composed of a cast iron flange, cement, and ceramic body, bonded with adhesive. According to statistics, more than 95% of fractured ceramic bottles occur between the flange and the first umbrella cluster, within 30 mm of the flange. Therefore, the primary detection area is defined as within the 30 mm range around the adhesive section of the cast iron flanges at both ends of the ceramic sleeve [14].

To investigate the impacts of different array element numbers, array element frequency, and element spacing on the imaging of subtle defects in the ceramic sleeve, a two-dimensional cross-sectional model of the ceramic sleeve, with an outer diameter of 80 mm and an inner diameter of 40 mm, was established using COMSOL finite element software. The model is coupled with the array elements via a coupling agent to ensure good coupling. Additionally, circular hole defects with a diameter of 1 mm were set at different positions within the ceramic sleeve to study the imaging effects of defects at various positions.

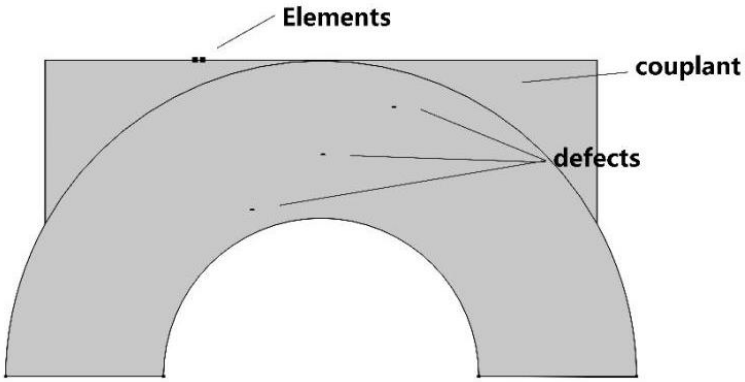

Figure 4: Finite Element Simulation Model of Ceramic Sleeve

When a single array element is used for excitation and reception, a snapshot of the acoustic field generated by the sound waves propagating within the ceramic sleeve is shown in Figure 5. Three circular hole defects are positioned at different locations within the ceramic sleeve. Due to the air-filled medium at the defect sites and the difference in acoustic impedance, the sound waves undergo reflection and transmission as they pass through the defects. The reflected sound waves propagate towards the upper boundary, while the transmitted sound waves continue towards the lower boundary [15]. At t = 0.92 μs, the array element begins to excite the ultrasound, which propagates from the element towards the interior of the workpiece. At t = 2.54 μs, the ultrasound reaches the positions of the first and second defects, and the reflected echo from the first defect has propagated close to the array element. At t = 3.95 μs, the reflected echoes from the first and second defects have also propagated near the upper surface array element, while the third defect experiences both reflection and transmission of ultrasound. Simultaneously, the ultrasound reaches the bottom surface, where the interface between air and ceramic creates reflected echoes from the bottom surface. At t = 6.18 μs, the bottom wave

reflection reaches near the probe surface, and the ultrasonic waves on both sides continue to propagate towards the lower part of the ceramic sleeve, gradually attenuating and eventually disappearing.

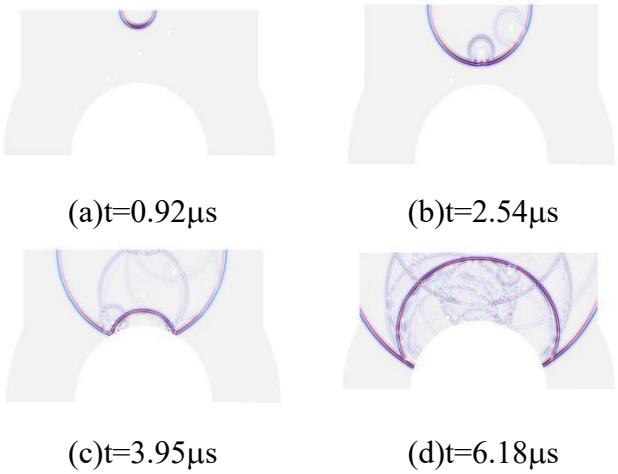

(a)t=0.92μs (b)t=2.54μs

(c)t=3.95μs (d)t=6.18μs

Figure 5: Snapshot of Sound Field Propagation in the Ceramic Sleeve

3.2 Influence of Array Element Number on TFM and PCI Imaging

As shown in Figure 6, the highlighted region at the top of the image represents the blind zone formed between the probe and the workpiece surface. The red arc at the bottom represents the bottom surface of the ceramic sleeve, with three prominent regions between the surface blind zone and the bottom wave, which correspond to the imaging of three air-hole defects.

The increase in the number of array elements leads to an extension of the total length of the array, thereby expanding the detection range [16]. However, for arc-shaped workpieces, the extension of the array length can result in poorer coupling effects. This means the air gap between the array elements and the workpiece will increase, which may cause greater attenuation of the ultrasound, thus degrading the detection image quality.

As the number of elements increases, the length and depth of both the surface blind zone and bottom surface also increase. For the 16-element detection image, due to the short probe length, the defect shapes on the left and right sides differ slightly from the actual round holes. The 32-element array provides better imaging, with defect shapes closer to the actual ones and lower background noise. For the 64-element array, the total length is longer, leading to poor coupling with the curved surface of the ceramic sleeve. As a result, some distortion occurs at the defect area, the surface blind zone increases, and background noise rises. Therefore, considering the overall imaging performance, the 32-element array provides the best imaging effect.

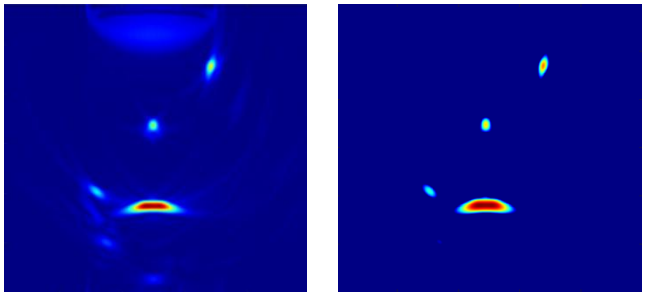

(a) 16-element

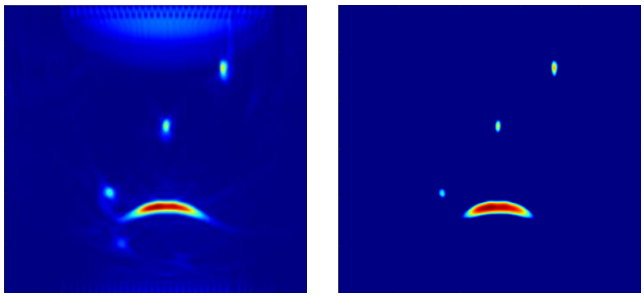

(b) 32- element

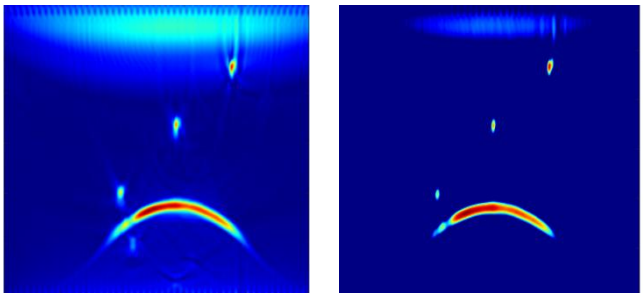

(c)64- element

Figure 6: TFM and PCI-dB Imaging with Different Numbers of Array Elements

3.3 Influence of Array Element Emission Frequency on TFM and PCI Imaging

In ultrasonic testing, increasing the frequency improves the ability to resolve defects. Resolution is generally considered to be half the wavelength of the ultrasonic wave. With the sound speed remaining constant, as frequency increases, the wavelength decreases, thereby improving the defect resolution capability[17, 18]. However, higher frequencies may also introduce more noise details. In practical applications, the frequency of the probe should be carefully selected based on the material's attenuation characteristics and specific resolution requirements.

From the results at 1, 3, and 5 MHz, it is observed that as the frequency increases, the image becomes clearer, and the accuracy of defect detection improves. Therefore, for detecting subtle defects inside the ceramic sleeve, the 5 MHz emission frequency is the optimal choice for defect detection.

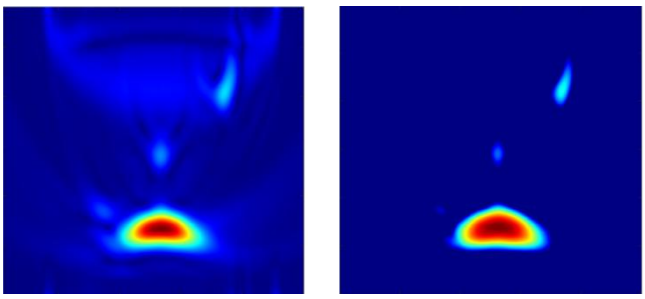

(a)1MHz

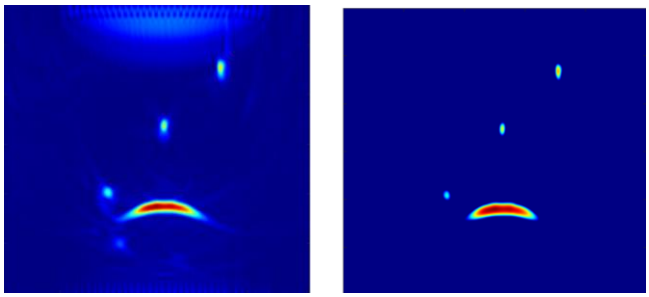

(b)3MHz

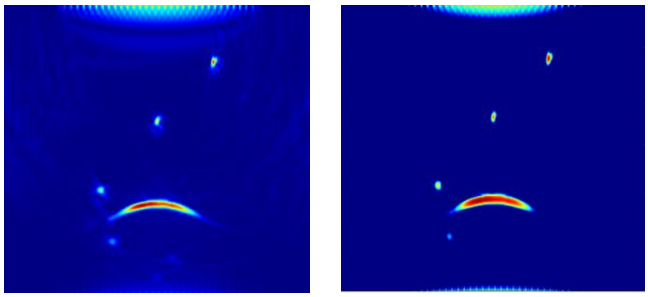

(c)5MHz

Figure 7: TFM and PCI-dB Imaging with Different Array Element Frequencies

3.4 Influence of Array Element Spacing on TFM and PCI Imaging

Increasing the spacing between array elements enhances the directionality of the array and broadens the detection area. However, if the element spacing is too large, grating lobes may occur [19]. Grating lobes, due to their high energy, are major contributors to artifact formation. Furthermore, increasing the element spacing also extends the total length of the array, which degrades coupling and causes greater ultrasound attenuation, leading to a poorer detection image. Therefore, the optimal element spacing in this study was set at 0.6 mm.

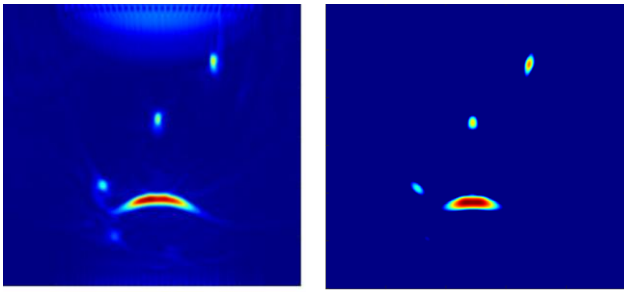

(a)0.6mm

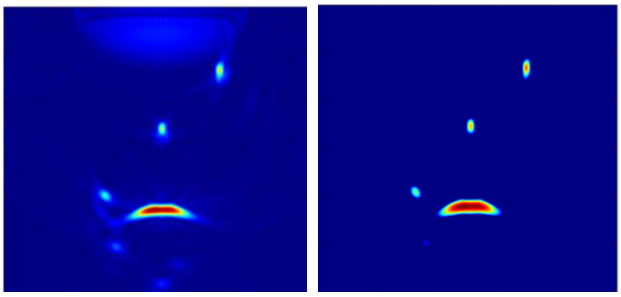

(b)0.8mm

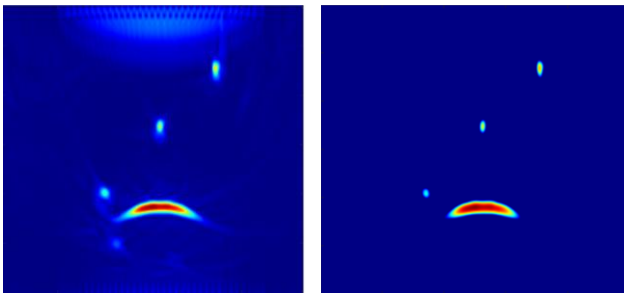

(c)1.0mm

Figure 8: TFM and PCI-dB Imaging with Different Array Element Spacings

4 Experimental Detection and Verification of Subtle Defects in Ceramic Sleeves

4.1 Ultrasonic Total-Focusing Detection of Ceramic Sleeve Defects

The ultrasonic total-focusing detection platform for ceramic sleeve defects is shown in Figure 9. It consists of a CTS-PA32BM phased array total-focusing imaging detection instrument, a flat-panel display, a phased array probe, a coupling agent, and ceramic sleeve samples. In the ceramic sleeve samples, air void defects with a diameter of 1mm are located at the near-surface, internal middle, and near-bottom positions. During the experiment, the probe filled with the coupling agent is directly placed on the ceramic sleeve surface. Under the effect of the coupling agent, ultrasonic waves are transmitted into the interior of the ceramic sleeve, achieving good coupling and reducing ultrasonic attenuation, which improves detection efficiency and accuracy. The reflected signals are then received by data transmission lines and sent to the flat-panel software. After organizing and analyzing the data, the reflected signals are converted into waveforms and images, which are displayed in the software.

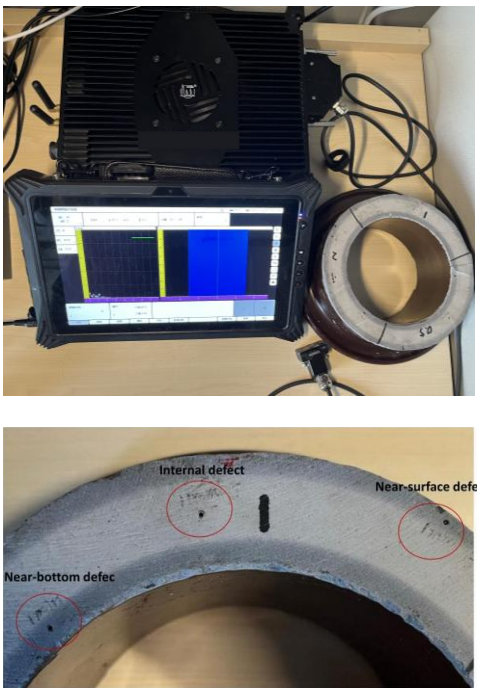

Figure 9: Ultrasonic Ceramic Sleeve Defect Detection Platform

4.2 Analysis of Near-Surface Defect Imaging in Ceramic Sleeves

The imaging of near-surface defects in the ceramic sleeve is shown below. The red-highlighted long strip at the lower-left corner of the image represents the bottom surface of the ceramic sleeve. Due to poor coupling, the position of the bottom wave is not directly beneath the probe. The area at the upper-middle of the image shows the imaging of the 1mm air void defect on the ceramic sleeve surface, while the rest of the image consists of noise and artifacts. Since the ceramic sleeve is an arc-shaped object, the ultrasonic wave propagation path inside is complex, and the probe cannot achieve good coupling with the surface of the ceramic sleeve. As a result, a significant amount of noise and artifacts appear in the image..

Due to the probe's inherent near-field detection limitation, near-surface defects are difficult to identify. Additionally, surface waves generated at the probe's contact with the ceramic sleeve interfere with the ultrasonic waves on the surface, which creats surface waves that disturb the detection signals in the near-surface region, making defect identification more challenging. As a result, the TFM image shows significant noise and artifacts near the surface, making it difficult to accurately identify defects. However, after phase-coherent denoising and dB amplitude enhancement processing, the noise and artifacts in the image are completely eliminated, and the TMF-PCI-dB image only displays the baseline waves and defects, making subtle defects in the ceramic sleeve more easily distinguishable.

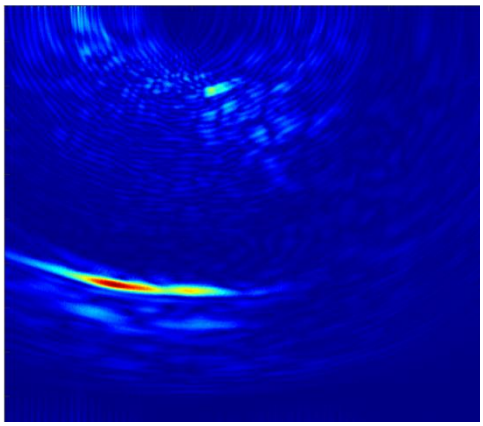

Figure 10: Defect TFM near the surface of the ceramic sleeve

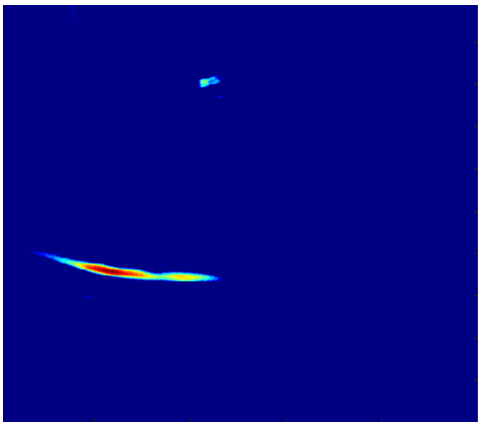

Figure 11: Defect TFM-PCI-dB near the surface of the ceramic sleeve

4.3 Analysis of Inner-Middle Defect Imaging in Ceramic Sleeves

The defect imaging of the inner middle section of the ceramic sleeve is shown below. The red-highlighted long strip at the bottom of the image represents the bottom surface of the ceramic sleeve. The area in the middle of the image corresponds to a 1mm pore defect in the inner middle section of the ceramic sleeve, while the rest of the image consists of noise and artifacts. Since the defect is not located near the surface, the TFM imaging of the defect in the inner middle section of the ceramic sleeve shows a significant reduction in noise and artifacts compared to the near-surface defects.

Although noise and artifacts are significantly reduced compared to near-surface defects, they are not completely eliminated. Some artifacts remain between the defect and the bottom wave. After phase-coherent denoising and dB amplitude enhancement processing, the noise and artifacts in the image are fully removed, greatly enhancing image accuracy.

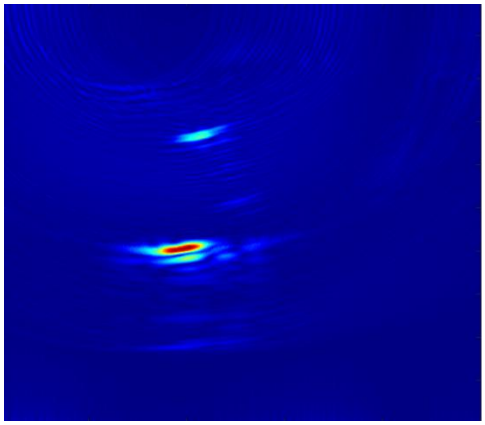

Figure 12: Defect TFM in the Inner Middle Section of the Ceramic Sleeve

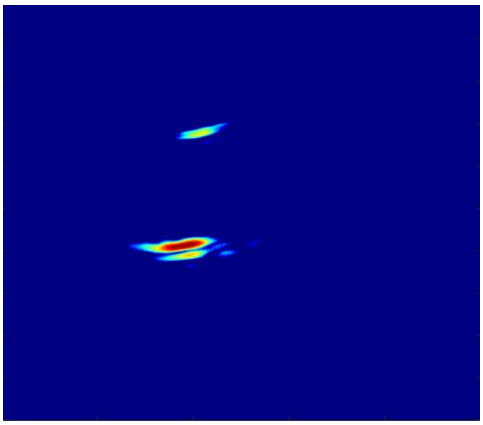

Figure 13: Defect TFM-PCI-dB in the Inner Middle Section of the Ceramic Sleeve

4.4 Analysis of Near-Bottom Defect Imaging in Ceramic Sleeves

The defect imaging of the near-bottom section in the ceramic sleeve is shown below. The red-highlighted long strip at the bottom of the image represents the bottom surface of the ceramic sleeve. The highlighted arc-shaped area above the bottom surface corresponds to the imaging of a 1mm pore defect near the bottom of the ceramic sleeve, with the rest of the image consisting of noise and artifacts. The noise and artifacts in this image are more prominent than those in the TFM image of the internal middle defect but less so than in the near-surface TFM image.

After phase-coherent denoising and dB amplitude enhancement processing, the noise and artifacts present in the defect imaging of the near-bottom section of the ceramic sleeve have been completely eliminated, significantly improving image precision and making subtle defects more distinguishable.

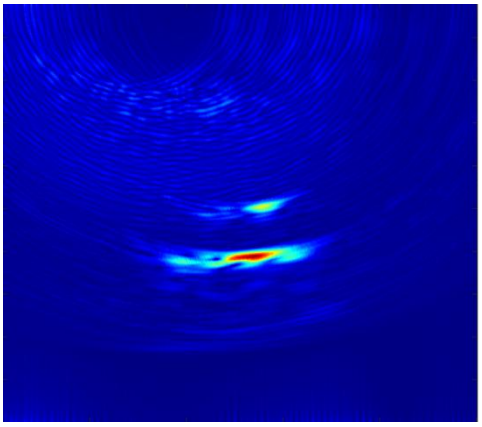

Figure 14: Defect TFM in the Inner Middle Section of the Ceramic Sleeve

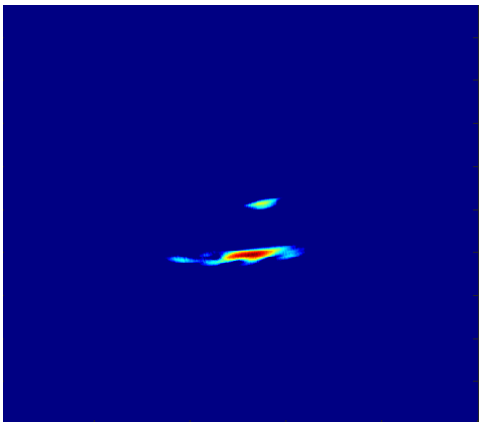

Figure 15: Defect TFM-PCI-dB in the Inner Middle Section of the Ceramic Sleeve

References

[1] Cai, C., Wang, Y. (2009). Experimental study on ultrasonic detection method for ceramic insulator sleeves. *Non-Destructive Testing*, 33(05), 11-15. (in Chinese)

[2] Jiang, Y., Wang, W. (2010). Ultrasonic testing technology for ceramic insulators and ceramic sleeves on live power grid supports. *East China Electric Power*, 38(10), 1566-1569. (in Chinese)

[3] Zong, F., Wan, S., Li, N., et al. (2021). Study on the influence of excitation-pickup distance on vibration detection of 220 kV ceramic pillar insulators. *Journal of Instruments and Instruments*, 42(10), 138-147. DOI: 10.19650/j.cnki.cjsi.J2108185. (in Chinese)

[4] Zhang, X., Li, J., Miao, X., et al. (2015). Longitudinal wave detection of ceramic insulators based on ultrasonic phased array technology. *Power Safety Technology*, 17(01), 57-61. (in Chinese)

[5] Qiu, G., Gao, C., Chen, J., et al. (2023). Research on real-time fault diagnosis of pillar ceramic insulators based on thermal imaging technology. *Insulating Materials*, 56(06), 100-105. DOI: 10.16790/j.cnki.1009-9239.im.2023.06.016. (in Chinese)

[6] Fan, X., Ma, S., Zhang, X., et al. (2014). Ultrasonic non-destructive testing and its application in the detection of electrical insulators. *High Voltage Apparatus*, 50(03), 109-114+119. DOI: 10.13296/j.1001-1609.hva.2014.03.020. (in Chinese) (in Chinese)

[7] Zhang, Y., & Li, X. (2020). Application of phase coherence imaging in ultrasonic array imaging using the total focusing method. In 2020 IEEE International Ultrasonics Symposium (IUS) (pp. 1-4). IEEE.

[8] Xu, N., Xu, L., He, F. (2023). Total-focusing imaging in anisotropic additive manufacturing components using ultrasonic array. *Journal of Beijing University of Aeronautics and Astronautics*, 49(5), 1063-1070. (in Chinese)

[9] Camacho, J., Fritsch, C., Fernandez-Cruza, J., et al. (2019). Phase coherence imaging: principles, applications, and current developments. *Proceedings of Meetings on Acoustics*, 178th Meeting of the Acoustical Society of America, San Diego, California. ASA.

[10] Chen, Y., Mao, Q., Shi, W., et al. (2019). Ultrasonic TOFD imaging inspection for heavy-walled weld based on phase coherence characteristics. *Journal of Mechanical Engineering*, 55(4), 25-32. (in Chinese)

[11] Mao, Q., Chen, Y., Shi, W., et al. (2020). Research on synthetic aperture focusing ultrasonic imaging based on phase coherence in the frequency domain. *Chinese Journal of Scientific Instrument*, 41(2), 135-145. (in Chinese)

[12] Kang, D., Chen, Y., Jin, S., et al. (2016). Enhancement of defect images in ultrasonic TOFD detection based on phase coherence imaging. *Pressure Vessel Technology*, 33(6), 59-66. (in Chinese)

[13] Chen, Y. (2016). Modeling of ultrasonic testing and noise suppression using phase coherence imaging algorithm in heavy-walled cast austenitic stainless steel. *Dalian: Dalian University of Technology*. (in Chinese)

[14] Li, Y., Qu, Y., Ding, J., et al. (2019). Analysis of the fracture cause of ceramic sleeves in 550 kV ceramic pillar circuit breaker arc extinguishing chambers. *High Voltage Apparatus*, 55(08), 249-252. DOI: 10.13296/j.1001-1609.hva.2019.08.036. (in Chinese)

[15] Smith, R. J., & Nelson, L. J. (2021). A comparative study of phase coherence imaging techniques in ultrasonic non-destructive testing. Ultrasonics, 114, 106415.

[16] Holmes, C., Brett, C. R., & Croxford, A. J. (2019). Enhanced defect characterization using phase coherence in total focusing method. NDT & E International, 103, 1-10.

[17] Zhang, H., Zhao, K. (2024). Research on ultrasonic phased array defect imaging and classification based on PCI-SVM. *Laser and Optoelectronics Progress*, 1-16. (in Chinese)

[18] Zhou, Y., Liu, Z., Liang, J., et al. (2024). Research on improved FFT algorithm in frequency domain total-focusing ultrasonic imaging. *Acta Metrologica Sinica*, 45(05), 722-729. (in Chinese)

[19] Yang, N., Lu, M., Zhang, P., et al. (2024). Total-focusing imaging of delamination defects in CFRP based on segmented ring array. *Journal of Instruments and Instruments*, 45(01), 200-210. DOI: 10.19650/j.cnki.cjsi.J2311973. (in Chinese)

[20] Liu, S., Zhu, Z., Hou, L., et al. (2023). Total-focusing imaging research of cracks in castings at different angles based on scattering information. *Foundry*, 72(12), 1591-1596. (in Chinese)

[21] Zhou, J., Zheng, Y., Zhang, Z., et al. (2017). Research on defect identification method based on partial scattering coefficient matrix. *Technical Acoustics*, 36(04), 335-339. DOI: 10.16300/j.cnki.1000-3630.2017.04.007. (in Chinese)